

Nonplanar tilts in very thin smectic films of one liquid-crystal compound

B. K. McCoy,^{1,2} Z. Q. Liu,^{1,3} S. T. Wang,⁴ Lidong Pan,¹ Shun Wang,¹ J. W. Goodby,⁵ and C. C. Huang¹

¹*School of Physics and Astronomy, University of Minnesota, Minneapolis, Minnesota 55455, USA*

²*Department of Mathematics and Physics, Azusa Pacific University, Azusa, California 91702, USA*

³*Department of Physics, Astronomy, and Engineering Science, St. Cloud State University, St. Cloud, Minnesota 56301, USA*

⁴*Department of Physics, Cornell University, Ithaca, New York 14853, USA*

⁵*Department of Chemistry, University of York, York YO10 5DD, United Kingdom*

(Received 10 February 2009; published 16 June 2009)

Surface effects cause tilted molecular arrangements in smectic layers near the surface of a free-standing liquid-crystal film in which the bulk of the film is in the smectic-A phase. One recent work has shown that the tilt directions in adjacent surface layers may be nonplanar. In this paper we study films with thicknesses of two to six smectic layers. Surface effects dominate in these very thin films. We show that the molecular tilts are nonplanar even in these very thin films.

DOI: [10.1103/PhysRevE.79.061702](https://doi.org/10.1103/PhysRevE.79.061702)

PACS number(s): 61.30.Hn, 64.70.M-, 77.84.Nh

I. INTRODUCTION

Many liquid crystals are interesting because they consist of molecules with elongated shapes. In various smectic-C (SmC) phases, molecular orientations are uniform within each layer, tilted at an angle θ away from the layer normal at an azimuthal angle φ [1]. The projection of the molecular axis on the layer plane is defined as the vector \vec{c} . Layer-to-layer variations in \vec{c} result in a variety of SmC phases with different electro-optical properties.

In smectic samples with free surfaces, the thermal fluctuations of layers are suppressed near the surface by surface tension, resulting in surface freezing [2]. This phenomenon is most easily observed when the bulk of a sample is in the smectic-A (SmA) phase. Several layers near the surface may contain tilted molecular arrangements, though the molecules are not tilted in the bulk. The tilt angle θ decreases exponen-

tially with distance away from the free surface with a correlation length on the order of a few layers [3]. Previous studies of free-standing films have shown that the tilt directions in the opposite sides of the film can be parallel or antiparallel. These arrangements are known as synclinic and anticlinic surfaces, respectively. These planar synclinic or anticlinic structures are by far the most common surface structures [4–10], though nonplanar tilts have been observed in opposite surfaces of a film [11] or within adjacent layers of a single surface [12,13]. Transitions between synclinic and anticlinic surfaces can be induced by changing the temperature [14,15] or applying an electric field [6,8,10] to the sample.

We have previously reported a series of five distinct surface structures in the bulk SmA temperature window of one chiral compound, (S)12OF1M7 [12]. The chemical structure of this compound is shown in Fig. 1. The bulk phase sequence for (S)12OF1M7 is

$$\text{SmC}_A^*(78.4 \text{ }^\circ\text{C}) \text{ SmC}_{F11}^*(81.1 \text{ }^\circ\text{C}) \text{ SmC}_{F12}^*(84.0 \text{ }^\circ\text{C}) \text{ SmC}^*(91.3 \text{ }^\circ\text{C}) \text{ SmC}_\alpha^*(92.4 \text{ }^\circ\text{C}) \text{ SmA}.$$

Using null transmission ellipsometry (NTE), we obtained the detailed tilt structure within the tilted surface layers for one film thickness. The surface structures were shown to be synclinic or anticlinic. In addition, within each surface the polarizations of adjacent layers were either ferroelectric or nearly antiferroelectric. Here we use the terms synclinic and anticlinic to refer to the parallel or antiparallel tilts in the outermost layers on opposite sides of a film and the terms ferroelectric and antiferroelectric to refer to the parallel or antiparallel tilts in adjacent layers within a single film surface. All five observed surface structures contained nonplanar surface layers. The sequence of surface transitions was identified as a re-entrant ferroelectric-antiferroelectric-ferroelectric transition and a simultaneous double re-entrant synclinic-anticlinic-synclinic-anticlinic transition. In this paper, we report the tilt structures for films of two to six layers

of the same compound, thin enough that no bulk is present. We find that the tilts are nonplanar even in these very thin films. This is an improvement over previous data analyses [16], in which only planar tilts were considered.

II. EXPERIMENTAL METHODS

Null transmission ellipsometry uses the optical properties of a liquid-crystal sample to probe the molecular orientations. Because the molecules are anisotropic, the index of refraction of the material differs for light with the electric field parallel or perpendicular to the molecular long axis. Typically the index of refraction along the molecular axis, denoted as n_e , is greater than the one perpendicular to the molecular axis, n_o . When polarized light is transmitted

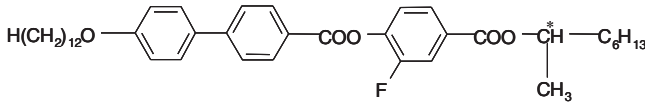


FIG. 1. Chemical structure of (S)12OF1M7.

through a film, the different indices of refraction cause a change in the polarization state. The polarization of the transmitted light depends on the relative orientations of the polarization of the incident light and the optical axis of the sample.

Details of our ellipsometer can be found in Ref. [17]. The null transmission state of the ellipsometer is defined by two ellipsometric parameters, Ψ and Δ . Ψ is the orientation of the analyzer axis. Δ is the phase lag between the \hat{p} and \hat{s} components of incident light necessary to produce linearly polarized transmitted light. One crucial feature of our ellipsometer is the capability of applying an electric field to the sample. The electric field is small, about 7 V/cm, and in the film plane. Each smectic layer has a ferroelectric polarization perpendicular to the tilt plane. The application of an external electric field causes the net polarization of the film to align parallel to the electric field. We can choose the direction of our applied field to be any direction within the film plane. This allows us to rotate the entire sample about the film normal, while the direction of the incident light remains constant. The angle between the electric field and the incident plane of the laser light is denoted as α , as shown in Fig. 2. By rotating the electric field, we can determine the rotational symmetry of the film. This in turn provides information about the arrangement of the molecular tilts.

In order to determine the molecular arrangements from the data, we use the 4×4 matrix method [18] to perform simulations. Each layer is modeled as an optically uniaxial medium, with the optical axis in the direction of the molecular axis. We obtained the indices of refraction $n_o = 1.496 \pm 0.003$ and $n_e = 1.658 \pm 0.003$ and the layer thickness $d = 3.66 \pm 0.05$ nm by the method described in Ref. [19]. Maxwell's equations are applied to find the transmitted electric and magnetic field vectors for a given incident beam for a single layer. This process is iterated to find the polarization of the transmitted beam through the entire sample. Given a model set of θ and φ for each layer, the simulations calculate values for the ellipsometric parameters Ψ and Δ .

III. THIN-FILM STRUCTURES

In very thin films, the entire film is affected by the surfaces so that no bulk SmA phase exists. We have previously

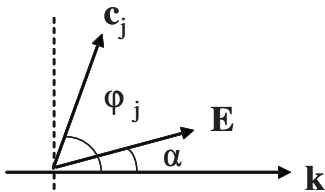


FIG. 2. Definition of angles used in the text. \mathbf{k} is the projection of the wave vector of the incident light on the film plane. \mathbf{E} is the direction of the applied electric field. \vec{c}_j is the \vec{c} vector of the j th layer.

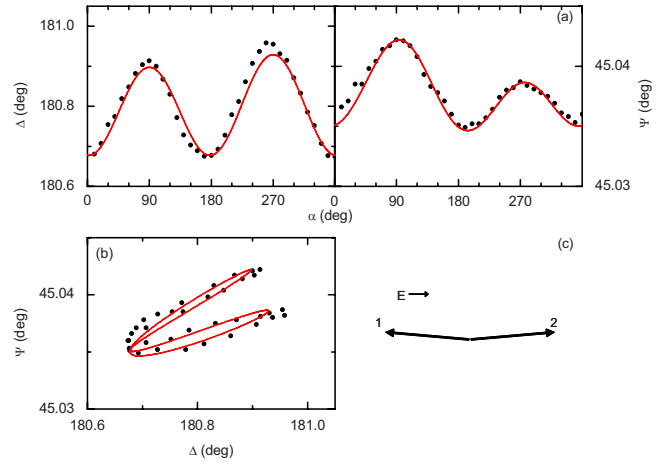


FIG. 3. (Color online) (a) shows the dependence of Δ and Ψ on α for a two-layer film at 100.1°C . (b) plots Ψ vs Δ . Circles are data and solid lines are simulation results. (c) shows the \vec{c} vectors used to obtain the simulations at $\alpha=0^\circ$.

determined that (S)12OF1M7 contains approximately three tilted layers at each surface when the bulk of the film is in the SmA phase [12,20]. We have studied films with thicknesses from two to six layers to see if the nonplanar structures observed in a 16 layer film persist when interior uniaxial layers are absent. Figure 3 shows the NTE data for a two-layer film at a temperature of 100.14°C . The Ψ vs α and Δ vs α curves have approximately 180° symmetry. This shows that the tilt structure within the film also has approximately 180° symmetry in rotation about the film normal. Since there are two layers, the film structure can be described by four angles: a tilt angle and an azimuthal angle for each layer. In this case, we assume that the film has symmetry about the central plane perpendicular to the film normal; the two layers have equal tilt angles. Only one of the azimuthal angles is a free parameter because the applied electric field determines the direction of the net polarization. Thus, there are only two free parameters: the tilt angle, θ , and the angle between the \vec{c} vectors of the first and second layers, $\varphi_1 - \varphi_2$. The azimuthal angles for the \vec{c} vectors of each layer are defined in Fig. 2. The solid lines in Fig. 3 show the results of a two parameter fit using the 4×4 matrix method. The simulation parameters are $\theta = 22 \pm 2^\circ$ and $\varphi_1 - \varphi_2 = 170 \pm 5^\circ$. A diagram showing the \vec{c} vectors for each layer is given in Fig. 3(c). It is interesting that the two tilts are not in the same plane in even this thin film. The existence of the smectic- C_α^* (Sm C_α^*) phase at a temperature lower than SmA in this compound may give rise to this nonplanar structure in two-layer films.

To fit the data for the three-layer film in Fig. 4, we used five parameters: three tilt angles and two azimuthal angles. The tilt angles of the outermost layers remain equal to within the uncertainty of our fits, but the middle layer has a slightly smaller tilt angle. The structure used for the simulations that best fit the data is shown in Fig. 4(c). The tilt angles are $\theta_1 = \theta_3 = 23 \pm 3^\circ$ and $\theta_2 = 22 \pm 5^\circ$. Only simulations in which the two outermost layers are in a nearly anticlinic arrangement adequately fit the data. The simulation shown in Fig. 4 uses angles of $\varphi_1 = 270 \pm 20^\circ$ and $\varphi_3 = 80 \pm 10^\circ$. The middle layer

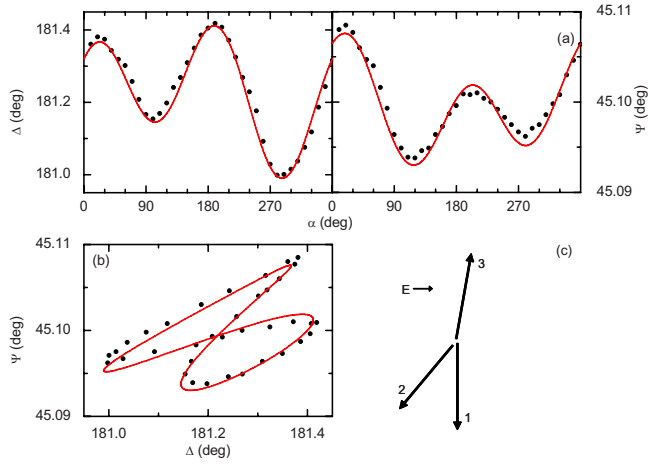


FIG. 4. (Color online) (a) shows the dependence of Δ and Ψ on α for a three-layer film at 100.2 °C. (b) plots Ψ vs Δ . Circles are data and solid lines are simulation results. (c) shows the \vec{c} vectors used to obtain the simulations at $\alpha=0^\circ$.

tilts in a different plane than the outermost layers. The angle between the tilt planes of the middle layer and the outer layers is $\varphi_1 - \varphi_2 = 40 \pm 20^\circ$. The angle between \vec{c}_1 and \vec{c}_2 is acute and the angle between \vec{c}_2 and \vec{c}_3 is obtuse. The simulation does not agree with the data if the middle layer of the model is rearranged so that the angle between \vec{c}_1 and \vec{c}_2 is obtuse and the angle between \vec{c}_2 and \vec{c}_3 is acute. Something breaks the symmetry between the top and bottom of the film. The film is a free-standing membrane stretched across a hole in a glass slide. The molecular chirality, anchoring of the film to the glass slide, or a small out-of-plane component of the applied electric field are candidates for breaking the symmetry between the top and bottom of the film.

The polarization of this three-layer film is also interesting. As mentioned previously, each layer has a ferroelectric polarization perpendicular to the tilt plane and the \vec{c} vector for the layer [1]. The net ferroelectric polarization is then perpendicular to the sum of the \vec{c} vectors for the film structure. Since the outermost layers tilt in nearly opposite directions, the polarizations of those layers nearly cancel, leaving the net ferroelectric polarization primarily due to the interior layer. However, the \vec{c} vector of the middle layer is not perpendicular to the applied electric field. Another contribution to the net polarization of the film comes from the flexoelectric polarization. In the continuum description, flexoelectric polarization [1,21] arises from gradients of the director \mathbf{n} , which points along the molecular long axis. In this three-layer film, we have spatial variations in the molecular axis, so a flexoelectric polarization is expected. The net polarization must be in the same direction as the electric field, so we can infer that the flexoelectric polarization has strength of the same order of magnitude as the ferroelectric polarization in this film.

The NTE data for a four-layer film and the associated simulations are shown in Fig. 5. The Ψ vs α and Δ vs α curves again show an anticlinic structure with $\varphi_1 = 180 \pm 4^\circ$ and $\varphi_4 = 0 \pm 4^\circ$. The differences between Ψ_{90} and Ψ_{270} and Δ_{90} and Δ_{270} are due to the inner layers. The simulations show that in order to obtain $\Psi_{90} > \Psi_{270}$ and $\Delta_{90} < \Delta_{270}$, the

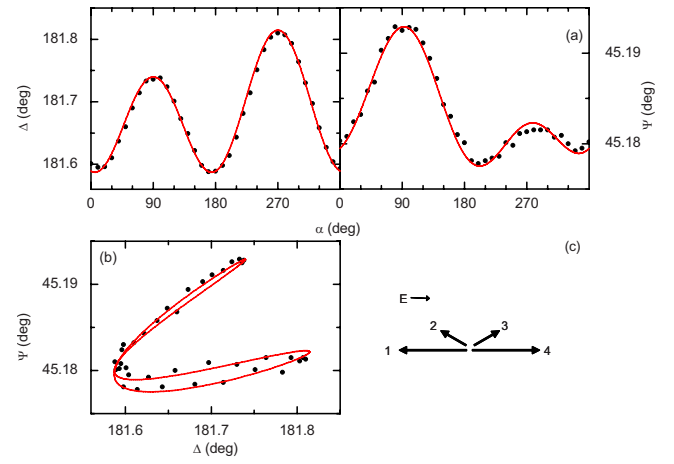


FIG. 5. (Color online) (a) shows the dependence of Δ and Ψ on α for a four-layer film at 103.1 °C. (b) plots Ψ vs Δ . Circles are data and solid lines are simulation results. (c) shows the \vec{c} vectors used to obtain the simulations at $\alpha=0^\circ$.

structure must have acute angles between the tilt planes of the first and second layers and the third and fourth layers. The simulation used tilt angles of the form

$$\theta_j = \theta_{\text{surf}} \frac{\cosh\left\{\left[2\left(j - \frac{1}{2}\right) - N\right]/2\xi\right\}}{\cosh([N-1]/2\xi)}. \quad (1)$$

Here j is the layer number, N is the total number of layers, and ξ is the tilt correlation length, with parameters $\theta_{\text{surf}} = 18.5 \pm 0.7^\circ$, $\xi = 0.92 \pm 0.12$ layers, and $\varphi_1 - \varphi_2 = \varphi_3 - \varphi_4 = 30 \pm 7^\circ$. The tilt angle in the outermost layers is smaller for this data than for the two-layer and three-layer films due to a higher temperature.

A five-layer film at 103.1 °C (Fig. 6) has a very similar

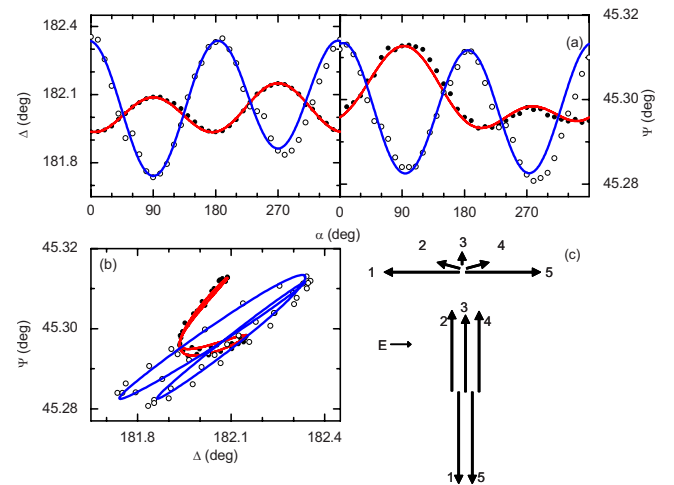


FIG. 6. (Color online) (a) shows the dependence of Δ and Ψ on α for a five-layer film at 103.1 °C (solid circles) and 90.7 °C (open circles). (b) plots Ψ vs Δ . Solid lines are simulation results. (c) shows the \vec{c} vectors used to obtain the simulations at temperatures 103.1 °C (top) and 90.7 °C (bottom).

structure to the four-layer film. The outermost layers are antclinic with angles of $\varphi_1=180\pm 4^\circ$ and $\varphi_5=0\pm 4^\circ$. The other simulation parameters are $\theta_{\text{surf}}=18.5\pm 0.5^\circ$, $\xi=0.82\pm 0.1$ layers, and $\varphi_1-\varphi_2=\varphi_4-\varphi_5=15\pm 10^\circ$. The primary difference between the four- and five-layer films is the addition of a middle layer in the five-layer film; the tilt plane in the middle layer lies halfway between the tilt planes of the second and fourth layers at $\varphi_3=90\pm 10^\circ$. It was previously noted that the three-layer film does not have reflection symmetry about the center of the film because of the nonplanar middle layer. One might also expect that other odd-layer films might not have reflection symmetry about the center of the film. Our fitting results for the five-layer film do have reflection symmetry. However, the middle layer has a tilt angle of $\theta_3=3.2\pm 0.1^\circ$; our simulations are less sensitive to the azimuthal orientations when the tilt angle is reduced, so we have a relatively large uncertainty in φ_3 and we cannot rule out asymmetry in this film. We expect asymmetry in the films to decrease as film thickness increases and the center layers are less affected by the surfaces.

Another important difference appears when varying temperature. The five-layer film undergoes a transition to another structure at 96.0°C , also shown in Fig. 6. In films of four layers or less, only one structure was observed per film at all temperatures. The minima of the Ψ vs α and Δ vs α curves occur at $\alpha=90^\circ$ and $\alpha=270^\circ$ at the lower temperature, while at higher temperature the minima occurred at $\alpha=0^\circ$ and $\alpha=180^\circ$. This indicates that the tilt plane for the outermost layers rotates by 90° . The structure for the five-layer film at low temperature changes to a synclinic arrangement of the outermost layers. The interior layers all tilt in the opposite direction of the outermost layers. The tilts for this structure are all planar. The simulation parameters are $\varphi_1=\varphi_5=270\pm 10^\circ$, $\varphi_2=\varphi_3=\varphi_4=90\pm 15^\circ$, $\theta_{\text{surf}}=22.5\pm 0.7^\circ$, and $\xi=3.32\pm 0.4$ layers. At this lower temperature, the tilt angle for the interior layers is much larger than at higher temperature due to an increase in the correlation length with decreasing temperature.

A six-layer film also has two structures depending on the temperature (Fig. 7). At 101.3°C , the structure is similar to the structure for a five-layer film above 96.0°C . The tilt angles for the simulation corresponding to the solid circles shown in Fig. 7 are $\theta_{\text{surf}}=18.1\pm 1.2^\circ$, with $\xi=0.82\pm 0.20$ layers. The azimuthal angles are $\varphi_1=180\pm 6^\circ$, $\varphi_2=145\pm 20^\circ$, $\varphi_3=145\pm 40^\circ$, $\varphi_4=35\pm 40^\circ$, $\varphi_5=35\pm 20^\circ$, and $\varphi_6=0\pm 6^\circ$. Figure 7 also shows a set of data for a six-layer film of the (R) enantiomer at 101.9°C . Switching the handedness of the compound also changes the handedness of the nonplanar tilts. In other words, the direction of $\vec{c}_1\times\vec{c}_2$ reverses. The direction of the ferroelectric polarization also changes with the handedness; for the (S) enantiomer, each layer has a polarization in the direction of $\vec{c}\times\hat{z}$, where \hat{z} is the layer normal, while for the (R) enantiomer, the polarization direction is $-\vec{c}\times\hat{z}$. Similar to the five-layer film, a six-layer film undergoes a transition to a synclinic structure as the temperature is lowered. The simulation at 92.2°C shown in Fig. 7 has tilt parameters of $\theta_{\text{surf}}=25.4\pm 2.0^\circ$ and $\xi=2.10\pm .45$ layers and azimuthal angles of $\varphi_1=\varphi_6=90\pm 8^\circ$, $\varphi_2=310\pm 10^\circ$, $\varphi_3=310\pm 15^\circ$, $\varphi_4=230\pm 15^\circ$, and $\varphi_5=230\pm 10^\circ$. Unlike the low-temperature structure in the five-layer film, this is a nonplanar structure.

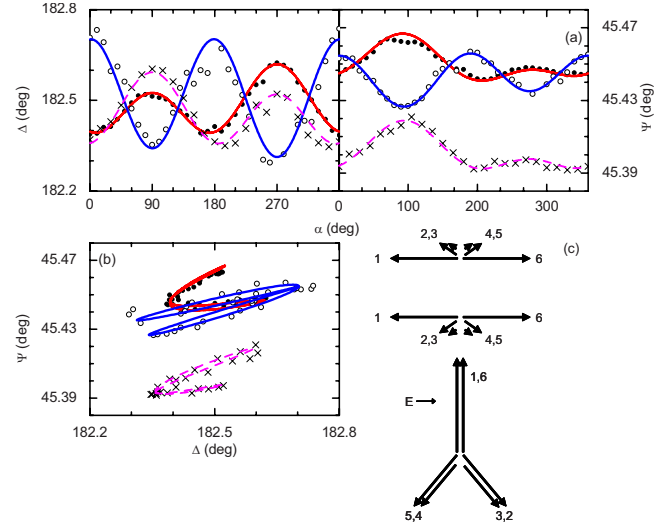


FIG. 7. (Color online) (a) shows dependence of Δ and Ψ on α for a six-layer film at 101.3°C (solid circles), 101.9°C for the (R) enantiomer (crosses), and 92.2°C (open circles). (b) plots Ψ vs Δ . Solid lines are simulation results. (c) shows the \vec{c} vectors used to obtain the simulations at $\alpha=0^\circ$ with temperatures 101.3°C (top), 101.9°C for the (R) enantiomer (middle), and 92.2°C (bottom).

In summary, for these very thin films we are able to determine the detailed film structure using NTE. Other nonplanar surface structures have previous been reported in a few antiferroelectric compounds. Chao *et al.* [14] showed that several surface transitions occur in smectic films of one antiferroelectric compound as thin as three layers. The surface transitions appear to be similar to the transitions studied in this paper, but the detailed tilt structure could not be determined by their calorimetric technique. Another antiferroelectric compound has been shown to have nonplanar surface tilts by Pan *et al.* for films as thin as 20 layers [13]. In this compound, synclinic surfaces with two ferroelectric surface layers evolve smoothly into antiferroelectric surface layers by rotation of the second layer. Our results have shown detailed measurements of the nonplanar tilt structures in films thin enough that there is no bulk SmA phase. Nonplanar tilts persist in films even as thin as two layers. Bulk samples of this compound exhibit the SmC_α^* phase at a temperature lower than the SmA phase. The SmC_α^* phase has been described by a model in which ferroelectric interactions between nearest-neighbor layers and antiferroelectric interactions between next-nearest-neighbor layers are frustrated [22,23]. The frustration causes the \vec{c} vectors in each layer to form a helical arrangement in the bulk SmC_α^* phase. The helical pitch at the SmA- SmC_α^* transition for this compound is 16 ± 1 layers [20], corresponding to an angle of 22.5° between the \vec{c} vectors of adjacent layers. It is interesting that this is approximately equal to $\varphi_1-\varphi_2$ for the high-temperature structures all of the films we studied except the two-layer film. We believe that the main origin of the observed nonplanar structures in very thin films is due to the existence of the SmC_α^* phase below the SmA phase in the bulk. We expect that nonplanar surface tilts are common in smectic films of antiferroelectric liquid-crystal compounds.

ACKNOWLEDGMENTS

This research was supported in part by the National Science Foundation, Solid State Chemistry Program under

Grants No. DMR-0106122 and No. DMR-0605760. B.K.M. and Z.Q.L. acknowledge support from the University of Minnesota Graduate School.

-
- [1] P. G. DeGennes and J. Prost, *The Physics of Liquid Crystals* (Clarendon, Oxford, 1993).
- [2] R. Holyst, Phys. Rev. A **44**, 3692 (1991).
- [3] Ch. Bahr, C. J. Booth, D. Fliegner, and J. W. Goodby, Phys. Rev. E **52**, R4612 (1995).
- [4] Ch. Bahr and D. Fliegner, Phys. Rev. Lett. **70**, 1842 (1993).
- [5] P. O. Andreeva, V. K. Dolganov, C. Gors, R. Fouret, and E. I. Kats, JETP Lett. **67**, 856 (1998).
- [6] D. R. Link, G. Natale, N. A. Clark, J. E. Maclennan, M. Walsh, S. S. Keast, and M. E. Neubert, Phys. Rev. Lett. **82**, 2508 (1999).
- [7] P. V. Dolganov, J. W. Goodby, and A. Seed, Eur. Phys. J. E **3**, 7 (2000).
- [8] P. M. Johnson, D. A. Olson, S. Pankratz, Ch. Bahr, J. W. Goodby, and C. C. Huang, Phys. Rev. E **62**, 8106 (2000).
- [9] B. Rovšek, M. Čepič, and B. Žekš, Phys. Rev. E **66**, 051701 (2002).
- [10] S. T. Wang, X. F. Han, Z. Q. Liu, A. Cady, M. D. Radcliffe, and C. C. Huang, Phys. Rev. E **68**, 060702(R) (2003).
- [11] X. F. Han, D. A. Olson, A. Cady, D. R. Link, N. A. Clark, and C. C. Huang, Phys. Rev. E **66**, 040701(R) (2002).
- [12] B. K. McCoy, Z. Q. Liu, S. T. Wang, V. P. Panov, J. K. Vij, J. W. Goodby, and C. C. Huang, Phys. Rev. E **73**, 041704 (2006).
- [13] L. D. Pan, S. Wang, C. S. Hsu, and C. C. Huang, Phys. Rev. E **79**, 031704 (2009).
- [14] C. Y. Chao, C. R. Lo, P. J. Wu, Y. H. Liu, D. R. Link, J. E. Maclennan, N. A. Clark, M. Veum, C. C. Huang, and J. T. Ho, Phys. Rev. Lett. **86**, 4048 (2001).
- [15] X. F. Han, S. T. Wang, A. Cady, M. D. Radcliffe, and C. C. Huang, Phys. Rev. Lett. **91**, 045501 (2003).
- [16] A. Fera, R. Opitz, W. H. de Jeu, B. I. Ostrovskii, D. Schlauf, and Ch. Bahr, Phys. Rev. E **64**, 021702 (2001).
- [17] D. A. Olson, X. F. Han, P. M. Johnson, A. Cady, and C. C. Huang, Liq. Cryst. **29**, 1521 (2002).
- [18] D. W. Berreman, J. Opt. Soc. Am. **62**, 502 (1972); H. Wohler, G. Haas, M. Fritsch, and D. A. Mlynski, *ibid.* **5**, 1554 (1988).
- [19] D. A. Olson, S. Pankratz, P. M. Johnson, A. Cady, H. T. Nguyen, and C. C. Huang, Phys. Rev. E **63**, 061711 (2001).
- [20] V. P. Panov, B. K. McCoy, Z. Q. Liu, J. K. Vij, J. W. Goodby, and C. C. Huang, Phys. Rev. E **74**, 011701 (2006).
- [21] A. V. Emelyanenko and M. A. Osipov, Phys. Rev. E **68**, 051703 (2003).
- [22] D. A. Olson, X. F. Han, A. Cady, and C. C. Huang, Phys. Rev. E **66**, 021702 (2002).
- [23] P. V. Dolganov, V. M. Zhilin, V. K. Dolganov, and E. I. Kats, Phys. Rev. E **67**, 041716 (2003).